

Full length article

Quantifying adhesion of ultra-thin multi-layer DLC coatings to Ni and Si substrates using shear, tension, and nanoscratch molecular dynamics simulations



Michael R. Price, Bart Raeymaekers*

Dept. of Mechanical Engineering, University of Utah, Salt Lake City, UT, 84112, USA

ARTICLE INFO

Article history:

Received 25 May 2017

Received in revised form

20 August 2017

Accepted 14 September 2017

Available online 15 September 2017

Keywords:

Nanoscratch

Molecular dynamics

Diamond-like carbon

Hard disk drive

Ultra-thin films

ABSTRACT

Ultra-thin diamond-like carbon (DLC) coatings are used in many engineering applications including hard disk drives, automobile engines, and MEMS/NEMS devices to protect delicate substrates against wear and corrosion. However, they are susceptible to brittle cracking and delamination due to high intrinsic stress and poor adhesion to many substrates. Inclusion of an intermediate layer can prevent delamination of the coating. We perform simple shear and tension loading and nanoscratch molecular dynamics simulations to quantify the effect of coating layer thickness and composition on the adhesion of the ultra-thin multi-layer DLC coatings used in hard disk drives to their substrate. We observe that an intermediate Si layer improves adhesion of DLC coatings to Ni substrates compared to coatings without one, and that an optimum thickness of the Si layer exists. We also find that an intermediate DLC layer with sp^3 fraction lower than the outermost DLC coating layer protects the substrate from plastic deformation under external loading, and that it improves adhesion to Si but not Ni substrates compared to coatings with no intermediate layer.

© 2017 Acta Materialia Inc. Published by Elsevier Ltd. All rights reserved.

Introduction

Ultra-thin (<10 nm) diamond-like carbon (DLC) coatings are often used to protect delicate substrates and structures from wear and corrosion, due to their high hardness, low coefficient of friction when sliding against a variety of materials, and chemical stability in a multitude of environments [1]. The mechanical properties of DLC are dependent on the fraction of sp^3 - and sp^2 -hybridized carbon-carbon bonds, which is controlled by the deposition process and allows tuning the coating's mechanical properties for a specific application [2]. As such, ultra-thin DLC coatings have been successfully employed in a myriad of engineering applications, including hard disk drives (HDDs) [3], medical devices [4], MEMS/NEMS devices [5], and internal combustion engines [6], among others. However, their effectiveness as a protective layer is limited by poor adhesion to many substrates due to high intrinsic residual stress [1], which leads to brittle fracture and delamination of the

DLC coating from the substrate under external loading [5]. A challenge in the design of ultra-thin DLC coatings is understanding how to prevent or reduce delamination as a function of design parameters, including coating and substrate composition and coating thickness.

Studies have quantified adhesion and delamination of DLC coatings in light of extending their longevity. A common experimental technique is the nanoscratch test, in which a hard indenter tip is moved tangentially across the surface under a constant or steadily increasing load until coating failure occurs [7]. Coating failure may occur as radial cracking, through-thickness cracking, permanent deflection of the coating, delamination, or a combination of these mechanisms, depending on the hardness of the coating and substrate, thickness of the coating, and chemical adhesion between coating and substrate [7,8]. Determining the mechanisms of coating failure and quantifying the adhesion strength of the coating to the substrate is accomplished by analyzing changes in the normal load, tangential load, indenter depth, and friction coefficient during the scratch, and by examining the surface of the coating after the scratch to determine the scratch

* Corresponding author.

E-mail address: bart.raeymaekers@utah.edu (B. Raeymaekers).

profile and the size, shape, and composition of any debris generated by the scratch. Nanoscratch tests show that failure of ultra-thin DLC coatings is determined primarily by the amount of plastic deformation in the substrate [9], which may lead to cracking and delamination of the coating [10,11]. Furthermore, adhesion of DLC coatings to the substrate depends on external load, residual stress in the coating, coating and substrate composition, and coating thickness [11–13].

Researchers have proposed a number of techniques to prevent, reduce, or postpone delamination of ultra-thin DLC coatings under external loading by reducing the residual stress in the DLC and improving adhesion of the DLC coatings to the substrate. Some of these techniques, such as carbon ion implantation into the substrate before coating deposition [14,15], modifying coating deposition parameters [16,17], doping the DLC [18–20], tuning the substrate temperature during deposition [21], and thermal annealing of coating and substrate after coating deposition [3,20] can change the mechanical properties of the coating and reduce its ability to protect the substrate. Furthermore, these techniques can directly damage the substrate through ion bombardment, melting, or increased diffusion between regions of different materials [3,14,16,17,20]. Thus, they are inadequate when such damage compromises the function of delicate substrate materials and nanostructures. Other techniques improve adhesion without affecting the mechanical properties of the DLC coating material or damaging the substrate, such as including nanocrystals of a metallic phase within the DLC coating [22–24], deposition of an intermediate layer between the DLC and the substrate [25–27], deposition of multiple, alternating layers of hard DLC and a softer material such as a metal or a softer DLC [26,28–30], or creating a composition gradient between the substrate and the DLC coating [26,31,32]. However, it is difficult to theoretically predict and experimentally determine how the different materials deform under external loading, and understand how that deformation leads to delamination. This is particularly true when the coatings are several nanometers thick and the deformation of the coating is dominated by atomic-scale effects.

Molecular dynamics (MD) simulations have been used to simulate deformation and adhesion of ultra-thin multi-layer coatings under combined normal and tangential loading. MD simulations of nanoscratch tests [33,34] and other normal and tangential loading cases [35–38] of DLC coatings provide descriptions of the change in atomic structure near the surface of the coating due to loading [33–35], the adhesion between the DLC coating and the contacting surface [36,37], and the friction coefficient during sliding [38]. However, these studies model either DLC only or a single-layer DLC coating on a substrate, and do not investigate adhesion of the DLC coating to the substrate. Other MD studies quantify adhesion between different materials or multiple layers in a coating, and find that MD correctly predicts the qualitative trends of adhesion strength between different materials [39–42]. However, the materials in these simulations are typically crystalline metals rather than amorphous DLC. No studies exist that evaluate atomic-scale deformation of an ultra-thin multi-layer DLC coating under combined normal and tangential loading, to provide design guidelines to minimize deformation and delamination of the DLC coating for a given set of loading conditions. Hence, the objective of this paper is to determine the effect of coating design parameters of an ultra-thin multi-layer DLC coating, including thickness and composition of the layers, on the adhesion of the coating to the substrate. This will provide an understanding of how ultra-thin multi-layer DLC coatings deform and separate from the substrate under external loading, and provide information on how to design DLC coatings to facilitate their use in engineering applications.

2. Methods

2.1. Model

We model the ultra-thin DLC coating of an HDD recording head, which contains an sp^3 -fraction of approximately 70% (i.e., tetrahedral amorphous carbon, ta-C [2]) and protects the magnetic read/write components from wear and delamination due to accidental contact with the disk. A Si, SiN, or Cr layer is often used on the recording head to improve adhesion between the DLC coating and the substrate material [25,43]. Increasing the storage density of HDDs requires decreasing the magnetic spacing between the recording head and the disk, which is accomplished in part by decreasing the thickness of the protective coatings.

Fig. 1 (a) shows a schematic of the head/disk interface of an HDD near the pole tip area of the recording head where wear and delamination have been experimentally observed [44]. This section of the recording head consists of the GMR element and write coils for reading and writing data, respectively, the magnetic shields and top pole, and the multi-layer protective DLC coating that consists of a DLC overcoat and intermediate Si layer. The magnetic disk consists of a substrate, the magnetic layer for storing data, a single-layer DLC overcoat, and a lubricant layer. The magnetic spacing is the distance between the magnetic layer of the disk and the GMR element and write coils of the head. Fig. 1 (b) shows the MD model of a small portion of the recording head, indicated by a red rectangle in Fig. 1 (a). The MD model consists of a Ni substrate of thickness t_{sub} and a multi-layer DLC coating consisting of a DLC layer of thickness t_1 and an amorphous Si (a-Si) layer of thickness t_2 . We model the top pole permalloy substrate material as Ni to simplify the computational model. Although the magnetic properties of permalloy and Ni are different, their mechanical properties including hardness, Young's modulus, Poisson's ratio, and lattice

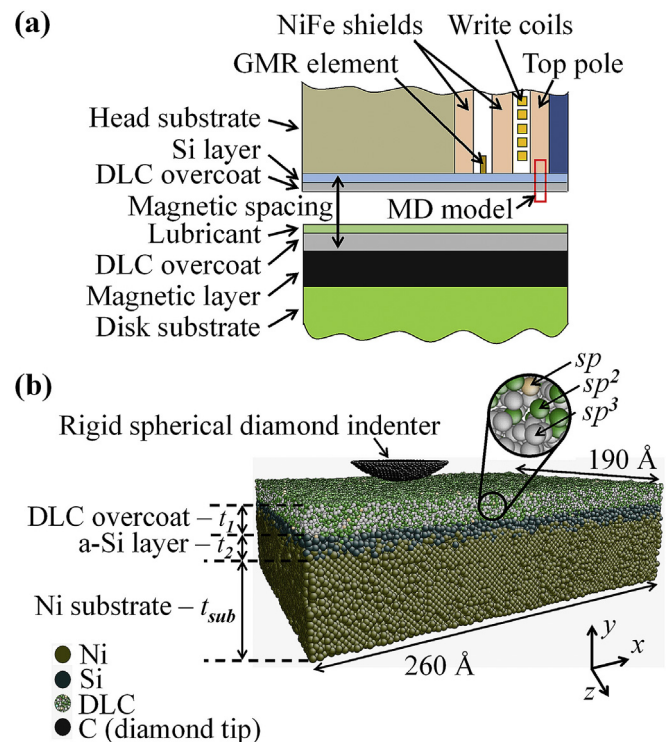


Fig. 1. (a) Schematic of a portion of the recording head and magnetic disk in an HDD. (b) MD model of a small portion of the recording head, indicated by the red rectangular box in (a).

structure are similar [45–48]. We model the rigid, spherical indenter with C atoms in a diamond lattice, and select the indenter tip radius of $r = 40 \text{ \AA}$ and simulation volume of $260 \times 100 \times 190 \text{ \AA}^3$ after a convergence study to ensure that boundary effects of the simulation box are negligible.

Fig. 2 shows a schematic of the four different combinations of coating and substrate materials used in this study. We vary the thickness and composition of the coating layers t_1 and t_2 to systematically investigate their effect on adhesion of the coating to the substrate, which we measure as the force required to separate the coating from the substrate under tension or shear loading. Coating type I is similar to the DLC coating on a recording head in an HDD (Fig. 1 (b)). We compare coating type I to type II to evaluate the effect of DLC sp^3 fraction on adhesion to the substrate. Coating types III-A and III-B are ta-C coatings on Ni and crystalline Si substrates, respectively, with a-C rather than a-Si as the material of the intermediate coating layer. We compare coating type III-A to type I to determine how adhesion of DLC coatings can be improved by modifying the properties of the DLC itself without the need for an intermediate layer of a different chemical composition, as observed by Logothetidis et al. [28] and Anders et al. [30]. Additionally, we replace the Ni substrate (type III-A) with crystalline Si (type III-B), a substrate commonly used in MEMS devices, to compare the effect of substrate material on the adhesion of DLC coatings as a function of coating layer thickness. DLC is known to display strong adhesion to Si and weak adhesion to Ni [13].

We vary the thickness of the coating layers, $12 \leq t_1 \leq 21 \text{ \AA}$ and $0 \leq t_2 \leq 9 \text{ \AA}$, while maintaining a constant total coating thickness of $t_1 + t_2 = 21 \text{ \AA}$, which is similar to the thickness of the protective coating on the recording head of an HDD. The substrate thickness t_{sub} remains 50 \AA throughout this work. We use the following interatomic potentials in the MD model: MEAM [39,49,50] for Ni–Ni, Ni–Si, and Ni–C interactions and Tersoff [51] for Si–Si, Si–C, and C–C interactions. For the C–C interactions between the indenter tip and the coating, we use a Morse potential parameterization that has previously been used to describe the interactions between a diamond indenter and substrate during nanoscratch simulations, with $D = 0.435 \text{ eV}$, $\alpha = 4.65 \text{ \AA}$, and $r_0 = 1.95 \text{ \AA}$ [52]. We overlap the MEAM and Tersoff potentials at the corresponding material interfaces to account for the many-body terms of the potentials. The model consists of approximately 330,000–450,000 atoms depending on coating thickness and composition. We use the Sandia LAMMPS code [53] for the MD simulations with a time step of 0.25 fs for all simulations.

We use a multi-step annealing procedure to create the MD model similar to the single-step annealing procedure used by others to create DLC [36,54]. We create a $260 \times 30 \times 190 \text{ \AA}^3$ block of DLC by heating diamond to 6000 K and rapidly quenching it, while

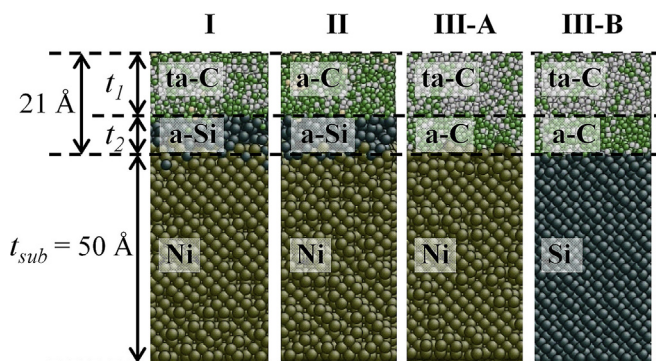


Fig. 2. Different combinations of coating and substrate materials used in this study.

controlling the pressure to tune the density and, thus, the sp^3 fraction of the DLC. We use a similar annealing procedure to create a block of a-Si. We merge the material blocks to create a single- or multi-layer coating ($t_2 = 0$ or $t_2 > 0$, respectively) on a substrate of crystalline Ni or Si, and perform the annealing procedure at the interface between the different material layers. We create coatings with layers of different thickness by removing atoms from the middle of each coating layer and annealing the layer back together. This procedure ensures that the atomic structure of the DLC coating surface and of the interfaces between material layers, including diffusion of atomic species into neighboring layers, are identical for all simulations. Thus, the simulation results are only dependent on the change in coating design parameters (e.g. layer thickness) and not on stochastic variation of the atomic structure at the material interfaces.

2.2. Simulation procedure

Fig. 3 shows the three different simulation procedures used in this work, including simple shear, simple tension, and nanoscratch simulations to quantify the effect of simple and combined normal and tangential loading on the adhesion of the coating to the substrate. Fig. 3 (a) illustrates the nanoscratch simulation procedure, similar to that used in other studies [55,56]. We press the indenter into the coating ($v_y = -50 \text{ m/s}$) until reaching an indentation energy of 2700 eV, identical for all nanoscratch simulations. We then translate the indenter tangentially across the coating over a distance of 84.5 \AA ($v_x = 50 \text{ m/s}$). Finally, we remove the indenter from the coating ($v_y = 50 \text{ m/s}$). 50 m/s is faster than what is typical for nanoindentation and nanoscratch experiments, but corresponds to the maximum relative velocity between the head and disk in a HDD

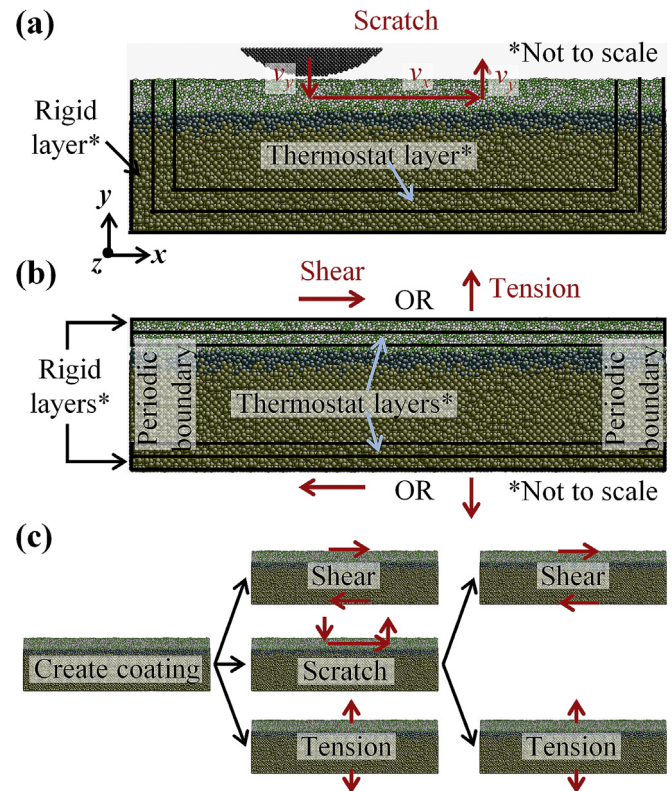


Fig. 3. (a) Nanoscratch simulation procedure. (b) Shear and tension simulation procedure. (c) Schematic of the process for performing shear, tension, and nanoscratch simulations for each coating.

[57]. Furthermore, 50 m/s falls within the range of indenter displacement rates used in other MD nanoscratch simulations, 20 m/s to 500 m/s (see e.g. Refs. [56,58–60]). Throughout the nanoscratch simulation, we hold the outer atomic layers along the sides and bottom of the simulation box rigid and maintain the next atomic layers inward at 300 K using a Langevin thermostat to simulate the bulk material around the simulation volume.

Fig. 3 (b) shows the simulation procedure for simulating simple tension and shear loading, similar to the procedure used in other MD studies [60–62]. We hold the outer atomic layers in the y -direction rigid at the top and bottom of the coating and substrate, respectively, and maintain the next atomic layers inward at 300 K using a Langevin thermostat. For tension loading simulations, we move the upper rigid section of the coating upward (50 m/s) until the coating has fully separated from the substrate. For the shear loading simulations, we move the upper rigid section of the coating 20 Å in the x -direction (50 m/s). Because the simulation box boundaries are periodic in the x - and z -directions, the shear loading simulations do not fully separate the coating from the substrate. In these cases, bonds between atoms that are broken due to shear loading can be replaced by bonds between different atoms.

Fig. 3 (c) shows a schematic of the process for performing simple shear, simple tension, and nanoscratch simulations for each coating of the desired coating composition and thickness. We perform independent shear, tension, and nanoscratch simulations on the coating, then perform second shear and tension simulations on the coating after it has undergone a nanoscratch simulation. A single scratch is insufficient to cause complete delamination of a DLC coating from the substrate, which typically only occurs after many cycles (see e.g. Ref. [63]). Hence, we compare the shear and tension simulation results before and after the nanoscratch simulation to evaluate which design parameters are most important in preventing damage that may lead to future delamination.

2.3. Data analysis

Fig. 4 shows a typical result of the x -force during shear loading and y -force during tension loading as a function of time for a ta-C and a-Si coating on a Ni substrate (type 1) with $t_2 = 3$ Å. Following an initial equilibration period, shear or tension of the coating begins. During shear simulations, the coating deforms until a maximum force F_{max} occurs at time t_{max} , at which point a shear band develops near the coating-substrate interface, the shear force decreases, and the coating begins to move in the x -direction. During tension simulations, the tension force decreases to zero after reaching F_{max} due to the complete separation of the coating from the substrate. Similar behavior is observed for all coatings. We

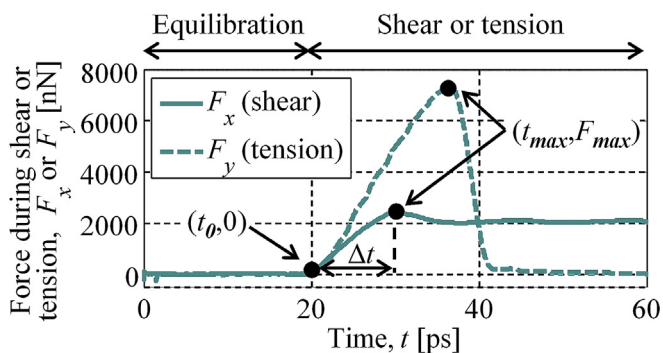


Fig. 4. x -force during shear and y -force during tension as a function of time, shown for a ta-C and a-Si coating on a Ni substrate (type 1) with an intermediate a-Si layer of thickness $t_2 = 3$ Å.

compare F_{max} under shear and tension loading for different coating designs to determine the effect of coating design parameters on a coating's resistance to shear and tension loading. We compare F_{max} under shear and tension loading for the same coating, before and after a nanoscratch simulation, to determine the effect of coating design parameters on deformation due to combined normal and tangential loading. We calculate the critical mean shear strain γ_{crit} , defined as the shear strain at the inception of coating separation during the shear simulations, as $\gamma_{crit} = v_x(\Delta t)/l_x$, where v_x is the shear velocity, Δt is the time until F_{max} is reached, and l_x is the length of the simulation box in the x -direction. We use γ_{crit} to evaluate the effect of coating design parameters on the local displacement required for coating separation and, thus, on the elasticity of the coating.

We quantify local shear strain by discretizing the simulation volume into grid elements and calculating a local average of the atomic bond rotation angle (ABRA). ABRA is a measure of the angle that a bond between two atoms has been rotated when atoms have been displaced due to loading, and is an indication of local shear strain [61]. Fig. 5 (a) shows a schematic of the three-dimensional simulation volume discretization technique we use to calculate the average ABRA within each grid element. Each bond that exists at the beginning and end of the simulation contributes to the average ABRA for the grid element in which the bond's midpoint is located. Two atoms are considered to be bonded when the distance between them is less than a cutoff determined using the first minimum in the radial distribution function for the given bond type [36,64], including Ni–Ni, Ni–Si, Ni–C, Si–Si, Si–C, and C–C bonds. Fig. 5 (b) shows a schematic of the one-dimensional simulation volume discretization technique that we use to quantify how properties including energy per atom, volume per atom, and bond length vary with coating depth and, thus, due to changes in layer composition and thickness.

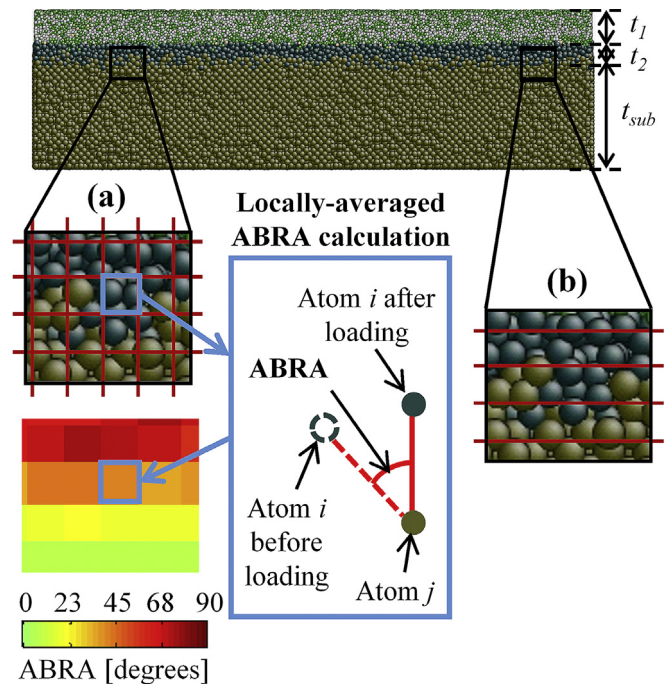


Fig. 5. Schematic of the three-dimensional simulation volume discretization technique for calculating local averages of ABRA. (b) 1-dimensional simulation volume discretization technique for quantifying how coating properties including energy per atom, volume per atom, and bond length vary with coating depth.

3. Results and discussion

We have simulated simple shear, simple tension, and nano-scratch procedures for the coatings shown in Fig. 2, to determine the effect of coating layer thickness and sp^3 fraction on the adhesion of the coating to the substrate, and plastic deformation of the substrate. Although we model a particular application of ultra-thin DLC coatings for HDDs, the results find use in a wide range of applications in which similar protective coatings are used.

We first evaluate the effect of coating composition, including thickness of an intermediate a-Si layer, and the sp^3 fraction of the DLC layer, on the adhesion of the DLC coating to the substrate, by determining the maximum force required to remove the coating from the substrate. Fig. 6 shows the force F_{max} to separate ta-C (70% sp^3 , type I) and a-C coatings (30% sp^3 , type II) from a Ni substrate under shear loading (dashed line) and tension loading (solid line), as a function of the thickness of the intermediate a-Si layer, t_2 . We observe that F_{max} is independent of the sp^3 fraction of the DLC layer over the range of parameters investigated. We also note that F_{max} is greater with an intermediate a-Si layer than without, and that for the coatings with an intermediate a-Si layer, F_{max} increases with decreasing intermediate layer thickness. This indicates that the presence of the a-Si layer improves the adhesion of DLC coatings to the Ni substrate, in agreement with the experimental observations by Holleck and Schier [65] and Li et al. [32]. Furthermore, the results indicate that an optimum thickness of the intermediate a-Si layer exists.

Fig. 7 shows the effect of the a-Si layer on the atomic structure of the Ni substrate near the coating-substrate interface to explain why the intermediate a-Si layer is critical for improving adhesion of a DLC coating to a Ni substrate. Fig. 7 (a) shows a close-up view of the coating-substrate interface for a ta-C coating (type I) without and with an intermediate a-Si layer ($t_2 = 0 \text{ \AA}$ and 3 \AA , respectively). The Ni lattice is less apparent near the interface with ta-C than near the interface with a-Si, indicating that the Ni atoms are further away from their equilibrium lattice positions in coatings without an intermediate a-Si layer compared to the coatings with an intermediate Si layer. This qualitative observation is quantified in Fig. 7 (b), which shows the deviation from equilibrium of the energy per Ni atom, volume per Ni atom (estimated using the Voronoi algorithm [66]), and Ni–Ni bond length as a function of depth into the Ni substrate for the coatings shown in Fig. 7 (a). We observe that the Ni substrate without an intermediate a-Si layer displays deviation from equilibrium ranging between -20% and 10% for energy per Ni

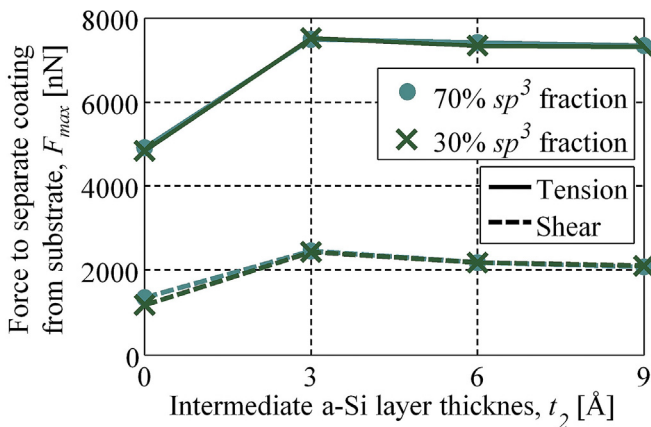


Fig. 6. Force to separate ta-C and a-C coatings from a Ni substrate (types I and II) under shear and tension loading as a function of the thickness of the intermediate a-Si layer, and the sp^3 fraction of the DLC coating.

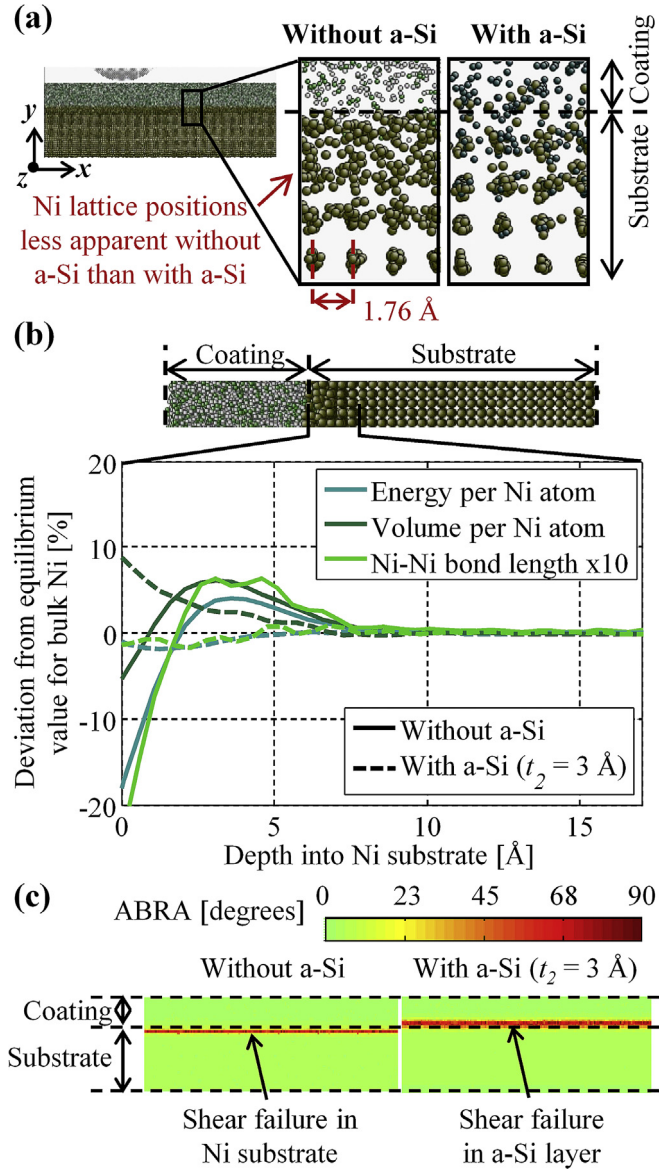


Fig. 7. (a) Close-up view of the coating-substrate interface for a ta-C coating without Si compared to with Si. (b) Deviation from equilibrium of the energy per Ni atom, volume per Ni atom, and Ni–Ni bond length as a function of depth into the Ni substrate for the coatings shown in (a). (c) Locally averaged ABRA for the coatings shown in (a).

atom, volume per Ni atom, and Ni–Ni bond length that penetrate $>7 \text{ \AA}$ into the substrate. Conversely, the Ni substrate with an intermediate a-Si layer shows deviation of $<3\%$ from equilibrium except in volume per Ni atom, which increases near the coating-substrate interface. This is due to the existence of a face-centered-cubic (FCC) phase of Ni_3Si with a Ni–Si bond length that differs from the Ni–Ni bond length of the FCC Ni substrate by 3.4% , which is much less than the $18\text{--}22\%$ difference between Ni–C and Ni–Ni bonds in their respective equilibrium atomic structures [39,50,67,68]. Thus, the presence of the intermediate a-Si layer causes the Ni lattice to be less distorted than when no intermediate a-Si layer is present.

Fig. 7 (c) shows the locally-averaged ABRA for the coatings shown in Fig. 7 (a) resulting from the shear loading described in Section 2.2. We observe permanent shear strain in the intermediate layer between Si atoms for all coatings with an intermediate a-Si layer, but in the substrate between Ni atoms for the coatings

without an intermediate a-Si layer. This corresponds to the location of maximum deviation from equilibrium in energy per Ni atom, volume per Ni atom, and Ni–Ni bond length (see Fig. 7 (b)). Therefore, coating failure without an intermediate a-Si layer occurs in the Ni substrate under lower shear and tensile loading than it would occur in an undistorted Ni lattice, or in the intermediate a-Si layer when it is present (see Fig. 6).

Fig. 8 shows a cross-section of the coating and substrate of a type I coating, and explains why the coatings with the thinnest intermediate a-Si have the greatest resistance to shear and tension loading (see Fig. 6). Fig. 8 (a) shows a snapshot of a typical shear simulation before and after shearing of a type I coating with $t_1 = 30 \text{ \AA}$ and $t_2 = 15 \text{ \AA}$. We show a coating with a thickness greater than 21 \AA for clarity of describing features that are not readily visible when $t_2 \leq 9 \text{ \AA}$. Atoms are colored as labeled in Fig. 1 (b) except for a thin band of atoms colored red according to their initial x -coordinate, to illustrate how each layer of the coating deforms due to shear loading. We observe that the Ni substrate and ta-C layer are unaffected by shear loading, but that the intermediate a-Si layer shows slip near the Ni–Si interface. Furthermore, the remainder of the intermediate a-Si layer has also plastically deformed, as evidenced by the positions of the red-colored atoms. Fig. 8 (b) shows the composition of the coating, the x -displacement of the atoms, and the normalized curvature of the x -displacement after shear loading, as a function of coating depth. The sheared region consists of the top atomic layers of the Ni substrate and the entire intermediate a-Si layer apart from the upper portion of the layer that is strengthened by the presence of C atoms. In addition, a critical shear region is defined as the atomic layers of the coating that slip with respect to the stationary substrate due to shear loading. The corresponding displacement Δx_{crit} increases at a rate approximately equal to the shear velocity once the coating is loaded beyond F_{max} . This critical shear region is bound by the global minimum and maximum in the normalized curvature of the x -displacement.

Fig. 8 (c) shows the distance between the coating-substrate interface and the top and bottom of the shear region and critical shear region as a function of the intermediate a-Si layer thickness. The distance between the top of the intermediate a-Si layer and the coating-substrate interface is also shown. We observe that the thickness of the shear region increases with increasing t_2 and that the thickness of the critical shear region is constant for all coatings investigated. Furthermore, we observe that the shear region and the critical shear region form increasingly deeper below the coating-substrate interface with decreasing t_2 and, thus, are comprised increasingly of Ni atoms rather than Si atoms. In the case of $t_2 = 0 \text{ \AA}$, failure under shear loading occurs entirely in the Ni substrate in the region that has been distorted by the Ni–C bonds due to the lack of a stable FCC phase of Ni and C (see Fig. 7). However, in the case of $t_2 = 3 \text{ \AA}$, the presence of an intermediate a-Si layer of even minimal thickness reduces the Ni lattice distortion at the coating-substrate interface. Thus, the penetration of the critical shear region into the substrate strengthens the critical shear region compared to coatings with $t_2 \geq 3 \text{ \AA}$, and the coating with $t_2 = 3 \text{ \AA}$ resists shear and tension loading best of all coatings we have evaluated (see Fig. 6). The critical shear region accounts for a decreasing portion of the total shear region with increasing t_2 , and the deformation of the coating under shear loading is increasingly dominated by the properties of a-Si itself and not by the surrounding materials. We observe that the location of coating separation during tension loading occurs at the same location within the coating in which the critical shear region occurs. Additionally, imperfections in the Ni lattice before loading such as dislocations or grain boundaries, which are not modeled in this study, reduce the stress necessary for plastic deformation in the Ni substrate.

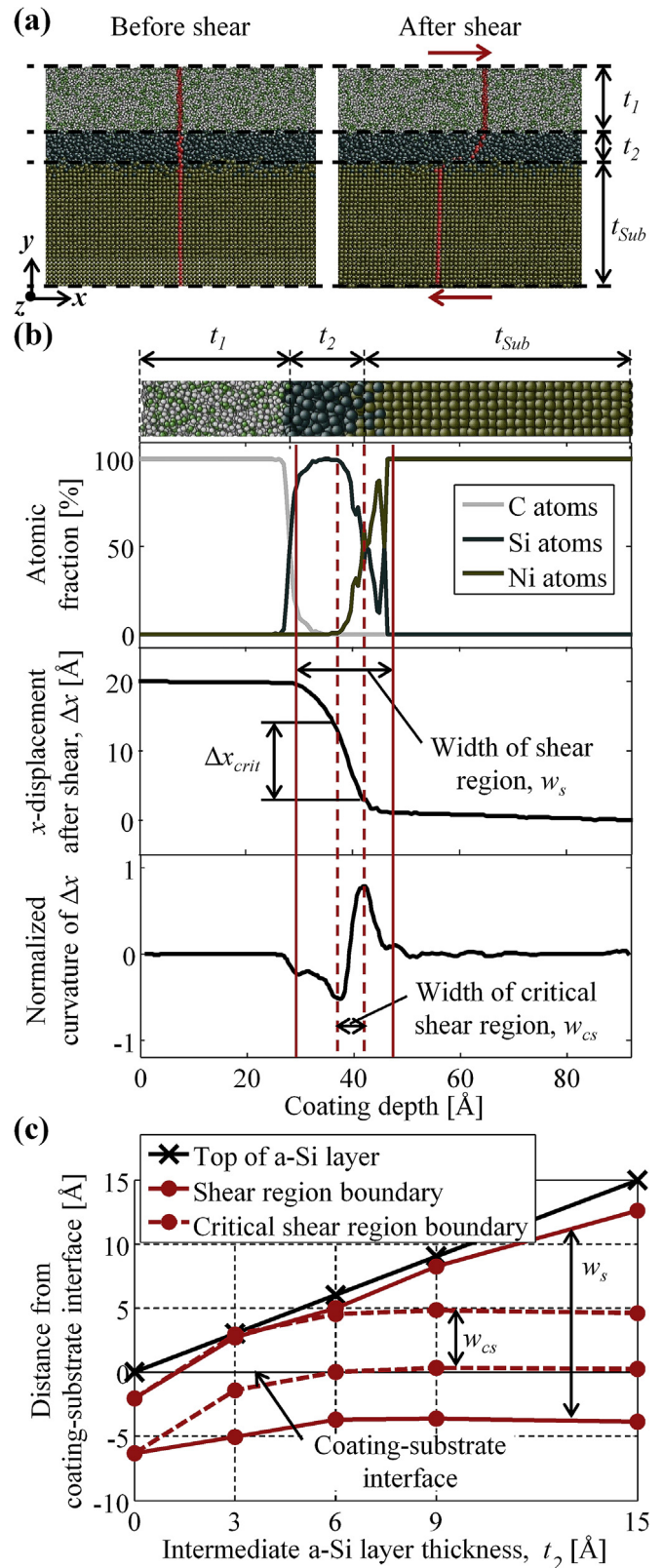


Fig. 8. (a) Snapshot of shear simulation before and after shearing a type I coating with $t_1 = 30 \text{ \AA}$ and $t_2 = 15 \text{ \AA}$. (b) Composition, x -displacement during shear, and curvature of x -displacement normalized by its maximum value as a function of coating depth. (c) Distance from coating-substrate interface of shear region and critical shear region as a function of intermediate a-Si layer thickness.

However, they are not expected to have significant effects on the qualitative behavior of local bonding between ta-C and Ni compared to a-Si and Ni observed in this study.

Continuum mechanisms, in addition to the atomistic mechanisms shown in Figs. 7 and 8, also play a role in the deformation of ultra-thin multi-layer DLC coatings and their ability to protect the substrate from plastic deformation. Increasing the thickness of an intermediate layer that has a lower hardness and stiffness than the ta-C layer reduces the hardness and stiffness of the entire multi-layer coating, as we previously documented in nanoindentation simulations of ultra-thin multi-layer DLC coatings [69]. This increases the deformation that occurs in the coating while reducing the deformation that occurs in the substrate and at the coating-substrate interface for a constant external load. Thus, increasing t_2 prevents damage to the substrate caused by an external load. Fig. 9 (a) shows the percent difference in critical mean shear strain γ_{crit} of a type I, II, or III coating compared to the critical mean shear strain in a coating of the same type without an intermediate a-Si or a-C layer as a function of intermediate layer thickness t_2 . We observe that γ_{crit} increases with increasing t_2 for all coating and substrate combinations evaluated. This is because the a-Si and a-C intermediate layer materials display lower stiffness than ta-C under shear and tension loading [70,71] and, thus, the stiffness of the coatings decreases with increasing t_2 . Similar behavior is observed for all coatings under tension loading. Fig. 9 (b) shows the percent weakening under shear loading after performing a nanoscratch simulation, as a function of intermediate layer thickness t_2 . Fig. 9 (c) shows before and after snapshots of the nanoscratch simulations for the cases indicated in Fig. 9 (b). We observe that the percent weakening under shear loading due to the scratch decreases with increasing t_2 , except for the type II coatings, for which a single scratch is insufficient to cause measurable damage with respect to separation of the coating from the substrate. Type II coatings, which consist of a-C and a-Si, are the softest and least stiff of the coatings evaluated and, thus, best protect the substrate and coating-substrate interface from plastic deformation, even without an intermediate a-Si layer, as observed in case C of Fig. 9 (c). This is in agreement with experimental results, which show that coating durability is increased with decreasing stiffness of the intermediate coating layer [63]. Indeed, the scratch slightly compresses the a-Si layer, which increases its density and results in a slight increase of F_{max} under shear loading after the scratch. For type I coatings, the presence of even 3 Å of a-Si is sufficient to protect the substrate from deformation such that no dislocations are emitted from the coating-substrate interface due to the scratch, which occurs without an intermediate a-Si layer as shown in case A of Fig. 9 (c). With the addition of a-C rather than a-Si as an intermediate layer, type III coatings with Ni substrates (III-A) do not entirely protect the substrate or coating-substrate interface from plastic deformation over the range of design parameters tested, although the percent weakening due to a scratch decreases with increasing thickness of the a-C layer. In nanoscratch simulations of a type III coating with Si substrate (III-B) we observe amorphization of the Si substrate near the coating-substrate interface, shown in case B of Fig. 9 (c), which weakens the coatings under both shear and tension loading. The amorphization of the substrate decreases with increasing thickness of the intermediate a-C layer, but we observe from Fig. 9 (b) that the case with $t_2 = 0$ Å is weakened less by the scratch than the case with $t_2 = 3$ Å. This cannot be explained using continuum theory, but is due to differences between the atomic structure of a-C and ta-C as described below. Furthermore, we note that while decreased hardness and stiffness of DLC coatings may help prevent or postpone delamination from the substrate, experimental studies have shown that the wear rate and friction coefficient of DLC coatings may increase with decreasing hardness and stiffness [72]. Thus, a

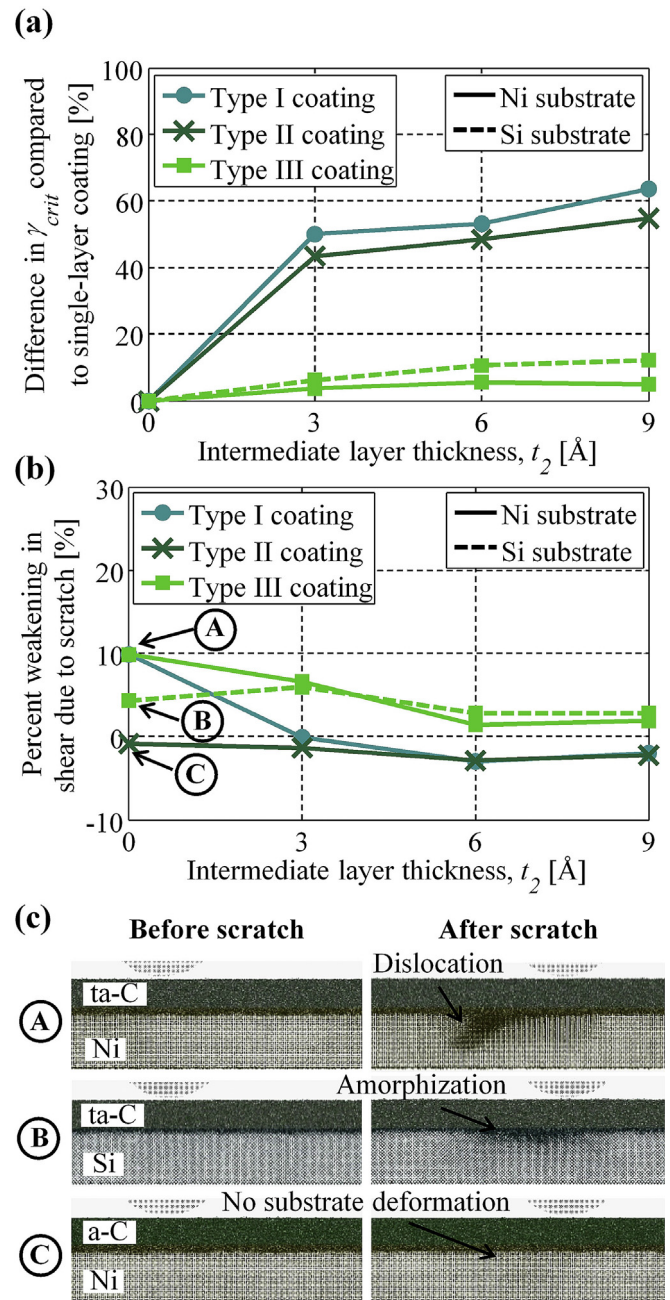


Fig. 9. (a) Percent difference in critical mean shear strain of type I, II, and III coatings compared to the critical mean shear strain in a single-layer coating of the same type as a function of intermediate layer thickness. (b) Percent weakening under shear loading due to a scratch as a function of intermediate layer thickness. (c) Snapshots of three nanoscratch simulations before and after the scratch for three cases labeled in (b).

balance must be found based on the design requirements and expected loading conditions of a particular coating. Maximizing the hardness of the outmost coating layer and using intermediate coating layer(s) to improve its adhesion to the substrate appears to be the best way to protect the substrate, similar to findings by Choy and Felix [73].

Fig. 10 (a) shows the difference between F_{max} of a type III coating and F_{max} of the same coating type without an intermediate a-C layer under shear and tension loading, as a function of the thickness of the intermediate a-C layer. We observe that the force required to separate the coating from the substrate under tension loading is

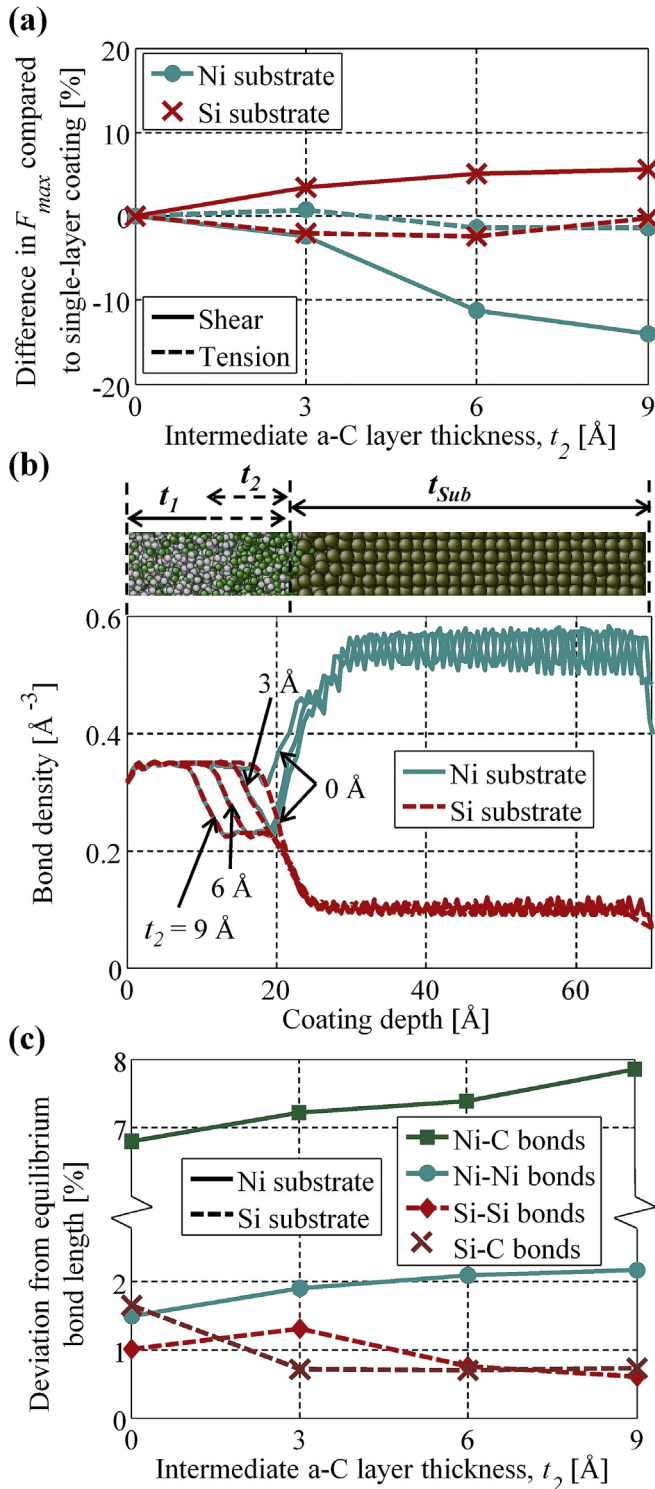


Fig. 10. (a) Difference between F_{max} of a type III coating and F_{max} of the same coating type without an intermediate a-C layer under shear and tension loading as a function of the thickness of the intermediate a-C layer. (b) Bond density in type III coatings as a function of coating depth. (c) Deviation from equilibrium of the bond lengths for the interfacial and substrate bonds within 5 Å of the coating-substrate interface for type III coatings before any external loading has been applied.

independent of the thickness of the intermediate a-C layer. However, we also observe that the force required to separate the coatings under shear loading increases with increasing t_2 for type III coatings on Si substrates (III-B) and decreases with increasing t_2 for

type III coatings on Ni substrates (III-A). Thus, although the a-C layer increases the elasticity of the coating and prevents damage to the substrate due to the scratch for all type III coatings (see Fig. 9), the presence of the a-C layer reduces the adhesion of ta-C to the Ni substrate under shear loading compared to the single-layer ta-C coating. This is due to differences in the atomic structure of the coating and substrate materials. Fig. 10 (b) shows the bond density in type III coatings as a function of coating depth. We observe that the bond density is greater in the ta-C layer compared to the a-C layer, due to the higher mass density and average coordination of C atoms in ta-C compared to a-C [2]. Furthermore, we observe that the bond density of ta-C is closer to that of Ni than Si and that the bond density of a-C is closer to that of Si than Ni. Thus, the local atomic structure near the interface is strained more to accommodate bonding between a-C and Ni than between ta-C and Ni, and is strained more to accommodate bonding between ta-C and Si than between a-C and Si. Fig. 10 (c) shows the deviation from equilibrium of the bond lengths for the interfacial (Ni-C and Si-C) and substrate (Ni-Ni and Si-Si) bonds within 5 Å of the coating-substrate interface for type III coatings (III-A and III-B, respectively) before any external loading has been applied. We observe that the Si-C bond length is independent of t_2 and the deviation from equilibrium of the Si-Si bond length decreases with increasing t_2 except for the case without intermediate a-C layer. In the case of $t_2 = 0$ Å the interfacial strain occurs between Si-C rather than Si-Si bonds. Thus, the substrate is stronger than it would be if the interfacial strain occurred between Si-Si bonds rather than Si-C bonds, and we observe less weakening in the amorphized Si substrate due to the scratch (see Fig. 9 (b)). We also observe that the Ni-Ni and Ni-C bonds show increasing deviation from their equilibrium bond length with increasing t_2 for type III-A coatings. Thus, the presence of the intermediate a-C layer weakens the adhesion between a ta-C coating and Ni substrate but strengthens that between a ta-C coating and Si substrate. Much experimental data has been obtained for coatings comprised of ta-C and a-C multi-layers on a Si substrate, which agrees qualitatively with the behavior we have observed for Si substrates [16,28,30,74–76]. Some authors have studied ta-C and a-C multi-layers on metallic substrates including stainless steel and Ti₆Al₄V [75,77], but a decrease in adhesion due to the presence of intermediate a-C layer(s) was not observed in these cases. However, the coatings are orders of magnitude thicker than the coatings in this study. Thus, the inclusion of an intermediate a-C layer may improve adhesion of ta-C to Ni substrates by reducing the stress in the coating [16] for thicker coatings and thus with higher intrinsic stress than the coatings modeled in this study.

4. Conclusions

We have performed simple shear and tension loading and nanoscratch simulations of ultra-thin multi-layer DLC coatings for a range of coating layer thicknesses and coating and substrate compositions including ta-C (70% sp^3 fraction DLC), a-C (30% sp^3 fraction DLC), and a-Si coating layers on crystalline Ni or Si substrates. We have determined the effect of the coating design parameters on the force required to separate the coating from the substrate under shear and tension loading both before and after a scratch and described the mechanisms by which different coating design parameters improve or degrade the adhesion between the coating and the substrate.

We conclude that the presence of an intermediate a-Si layer is critical for improving adhesion of ta-C and a-C coatings to Ni substrates. The bonding between Ni and C atoms at the coating-substrate interface forces the Ni atoms near the interface away from their equilibrium lattice positions and lowers the force

necessary to separate layers of Ni atoms in the distorted lattice compared to an undistorted lattice when subjected to shear and tension loading. Thus, DLC coatings without an intermediate a-Si layer fail below the DLC coating in the Ni substrate under both shear and tension loading. Si and Ni form a stable FCC phase near the interface, and bonding of the Si and Ni atoms causes minimal distortion of the Ni lattice. Failure occurs in the intermediate a-Si layer rather than a distorted Ni substrate, and the force necessary to separate the coating from the substrate under shear and tension loading increases when compared to coatings without an intermediate a-Si layer.

Furthermore, we conclude that there is an optimal thickness of the intermediate a-Si layer for improving adhesion of ta-C coatings on Ni substrates. The a-Si layer is softer than the ta-C layer and the Ni substrate, thus plastic deformation of the a-Si layer during shear loading, tension loading, and scratching increases with increasing thickness of the intermediate a-Si layer. Minimizing the thickness of the intermediate a-Si layer minimizes the amount of a-Si available to plastically deform and forces the critical failure region under shear and tension loading further into the substrate. This increases the force necessary to separate the coating from the substrate, provided enough Si is present to bond to the substrate in place of the DLC and, thus, prevent distortion of the Ni lattice.

We also conclude that decreasing the hardness and stiffness of the coating by increasing the fraction of the coating comprised of a-Si or a-C and decreasing the fraction comprised of ta-C increases the maximum strain observed in the coating during separation of the coating from the substrate under shear and tensile loading and protects the substrate from damage caused by a scratch. However, the adhesion between the coating and the substrate measured during shear loading as the shear force necessary to separate the coating from the substrate, depends on the atomic structure of the coating and substrate materials. Thus, an intermediate a-C layer improves adhesion of ta-C coatings to Si substrates but not to Ni substrates because the bond density of FCC Ni more closely matches that of ta-C than a-C, and that of crystalline Si more closely matches that of a-C than ta-C.

Acknowledgements

The authors thank Western Digital Corporation for their support of this research. The support and resources from the Center for High Performance Computing at the University of Utah are gratefully acknowledged. This work used the Extreme Science and Engineering Discovery Environment (XSEDE) [78], which is supported by National Science Foundation grant number ACI-1548562. We also acknowledge use of AtomEye [79].

References

- [1] C.A. Charitidis, Nanomechanical and nanotribological properties of carbon-based thin films: a review, *Int. J. Refract. Met. Hard Mater* 28 (2010) 51–70, <http://dx.doi.org/10.1016/j.ijrmhm.2009.08.003>.
- [2] J. Robertson, Diamond-like amorphous carbon, *Mater. Sci. Eng. R. Rep.* 37 (2002) 129–281, [http://dx.doi.org/10.1016/S0927-796X\(02\)00005-0](http://dx.doi.org/10.1016/S0927-796X(02)00005-0).
- [3] M.J. Carey, S. Maat, S. Chandrashekari, J.A. Katine, W. Chen, B. York, J.R. Childress, Co₂MnGe-based current-perpendicular-to-the-plane giant-magnetoresistance spin-valve sensors for recording head applications, *J. Appl. Phys.* 109 (2011) 93912, <http://dx.doi.org/10.1063/1.3563578>.
- [4] G. Dearnaley, J.H. Arps, Biomedical applications of diamond-like carbon (DLC) coatings: a review, *Surf. Coating. Technol.* 200 (2005) 2518–2524, <http://dx.doi.org/10.1016/j.surfcoat.2005.07.077>.
- [5] A. Erdemir, C. Donnet, Tribology of diamond-like carbon films: recent progress and future prospects, *J. Phys. D. Appl. Phys.* 39 (2006) R311–R327, <http://dx.doi.org/10.1088/0022-3727/39/18/R01>.
- [6] R. Hauert, An overview on the tribological behavior of diamond-like carbon in technical and medical applications, *Tribol. Int.* 37 (2004) 991–1003, <http://dx.doi.org/10.1016/j.triboint.2004.07.017>.
- [7] R. Jacobs, J. Meneve, G. Dyson, D.G. Teer, N.M. Jennett, P. Harris, J. von Stebut, C. Comte, P. Feuchter, A. Cavaleiro, H. Ronkainen, K. Holmberg, U. Beck, G. Reiners, C.D. Ingelbrecht, A certified reference material for the scratch test, *Surf. Coating. Technol.* 174–175 (2003) 1008–1013, <http://dx.doi.org/10.1016/S0257-8972>.
- [8] S.J. Bull, E.G. Berasetegui, An overview of the potential of quantitative coating adhesion measurement by scratch testing, *Tribol. Int.* 39 (2006) 99–114, [http://dx.doi.org/10.1016/S0167-8922\(06\)80043-X](http://dx.doi.org/10.1016/S0167-8922(06)80043-X).
- [9] T.H. Zhang, Y. Huan, Nanoindentation and nanoscratch behaviors of DLC coatings on different steel substrates, *Compos. Sci. Technol.* 65 (2005) 1409–1413, <http://dx.doi.org/10.1016/j.compscitech.2004.12.011>.
- [10] L.Y. Huang, K.W. Xu, J. Lu, B. Guelorget, Nano-scratching process and fracture mechanism of amorphous carbon films, *Wear* 254 (2003) 1032–1036, [http://dx.doi.org/10.1016/S0043-1648\(03\)00309-0](http://dx.doi.org/10.1016/S0043-1648(03)00309-0).
- [11] X.G. Ma, K. Komvopoulos, D. Wan, D.B. Bogy, Y.S. Kim, Effects of film thickness and contact load on nanotribological properties of sputtered amorphous carbon thin films, *Wear* 254 (2003) 1010–1018, [http://dx.doi.org/10.1016/S0043-1648\(03\)00307-7](http://dx.doi.org/10.1016/S0043-1648(03)00307-7).
- [12] P. Bruno, G. Cicala, A.M. Losacco, P. Decuzzi, Mechanical properties of PECVD hydrogenated amorphous carbon coatings via nanoindentation and nano-scratching techniques, *Surf. Coating. Technol.* 180–181 (2004) 259–264, <http://dx.doi.org/10.1016/j.surfcoat.2003.10.035>.
- [13] N. Yasui, H. Inaba, K. Furusawa, M. Saito, N. Ohtake, Characterization of head overcoat for 1 Tb/in² magnetic recording, *IEEE Trans. Magn.* 45 (2009) 805–809, <http://dx.doi.org/10.1109/TMAG.2008.2010636>.
- [14] W.J. MoberlyChan, D.P. Adams, M.J. Aziz, G. Hobbler, T. Schenkel, Fundamentals of focused ion beam nanostructural processing: below, at, and above the surface, *MRS Bull.* 32 (2007) 424–432, <http://dx.doi.org/10.1557/mrs2007.66>.
- [15] P.W. Shum, Z.F. Zhou, K.Y. Li, Optimisation of carbon implantation pre-treatments on the adhesion strength of amorphous carbon coatings on AISI 440C steel substrates, *Surf. Coating. Technol.* 166 (2003) 213–220, [http://dx.doi.org/10.1016/S0257-8972\(02\)00820-4](http://dx.doi.org/10.1016/S0257-8972(02)00820-4).
- [16] M. Gioti, S. Logothetidis, C. Charitidis, Stress relaxation and stability in thick amorphous carbon films deposited in layer structure, *Appl. Phys. Lett.* 73 (1998) 184–186, <http://dx.doi.org/10.1063/1.121749>.
- [17] P.J. Fallon, V.S. Veerasamy, C.A. Davis, J. Robertson, G.A.J. Amaratunga, W.I. Milne, J. Koskinen, Properties of filtered-ion-beam-deposited diamond-like carbon as a function of ion energy, *Phys. Rev. B* 48 (1993) 4777–4782, <http://dx.doi.org/10.1103/PhysRevB.48.4777>.
- [18] F. Zhao, H.X. Li, L. Ji, Y.F. Mo, W.L. Quan, H.D. Zhou, J.M. Chen, Structural, mechanical and tribological characterizations of a-C:H:Si films prepared by a hybrid PECVD and sputtering technique, *J. Phys. D. Appl. Phys.* 42 (2009) 165407, <http://dx.doi.org/10.1088/0022-3727/42/16/165407>.
- [19] M. Chhowalla, Y. Yin, G.A.J. Amaratunga, D.R. McKenzie, T. Frauenheim, Highly tetrahedral amorphous carbon films with low stress, *Appl. Phys. Lett.* 69 (1996) 2344, <http://dx.doi.org/10.1063/1.117519>.
- [20] A.C. Ferrari, B. Kleinsorge, N.A. Morrison, A. Hart, V. Stolojan, J. Robertson, Stress reduction and bond stability during thermal annealing of tetrahedral amorphous carbon, *J. Appl. Phys.* 85 (1999) 7191, <http://dx.doi.org/10.1063/1.370531>.
- [21] W.-J. Wu, M.-H. Hon, The effect of residual stress on adhesion of silicon-containing diamond-like carbon coatings, *Thin Solid Films* 345 (1999) 200–207, [http://dx.doi.org/10.1016/S0040-6090\(98\)01052-9](http://dx.doi.org/10.1016/S0040-6090(98)01052-9).
- [22] Y. Pauleau, F. Thiéry, V.V. Uglov, V.M. Anishchik, A.K. Kuleshov, M.P. Samtsov, Tribological properties of copper/carbon films formed by microwave plasma-assisted deposition techniques, *Surf. Coating. Technol.* 180–181 (2004) 102–107, <http://dx.doi.org/10.1016/j.surfcoat.2003.10.028>.
- [23] Y. Pauleau, F. Thiéry, Deposition and characterization of nanostructured metal/carbon composite films, *Surf. Coating. Technol.* 180–181 (2004) 313–322, <http://dx.doi.org/10.1016/j.surfcoat.2003.10.077>.
- [24] A.A. Voevodin, J.S. Zabinski, Supertough wear-resistant coatings with “chameleon” surface adaptation, *Thin Solid Films* 370 (2000) 223–231, [http://dx.doi.org/10.1016/S0040-6090\(00\)00917-2](http://dx.doi.org/10.1016/S0040-6090(00)00917-2).
- [25] C. Srisang, P. Asanithi, K. Siangchaew, A. Pokaipisit, P. Limsuwan, Characterization of SiC in DLC/a-Si films prepared by pulsed filtered cathodic arc using Raman spectroscopy and XPS, *Appl. Surf. Sci.* 258 (2012) 5605–5609, <http://dx.doi.org/10.1016/j.apsusc.2012.02.036>.
- [26] A.A. Voevodin, S.D. Walck, J.S. Zabinski, Architecture of multilayer nanocomposite coatings with super-hard diamond-like carbon layers for wear protection at high contact loads, *Wear* 203–204 (1997) 516–527, [http://dx.doi.org/10.1016/S0043-1648\(96\)07425-X](http://dx.doi.org/10.1016/S0043-1648(96)07425-X).
- [27] K.W. Chen, J.F. Lin, The study of adhesion and nanomechanical properties of DLC films deposited on tool steels, *Thin Solid Films* 517 (2009) 4916–4920, <http://dx.doi.org/10.1016/j.tsf.2009.03.124>.
- [28] S. Logothetidis, S. Kassavetis, C. Charitidis, Y. Panayiotatos, A. Laskarakis, Nanoindentation studies of multilayer amorphous carbon films, *Carbon* N. Y. 42 (2004) 1133–1136, <http://dx.doi.org/10.1016/j.carbon.2003.12.054>.
- [29] J. Meneve, E. Dekempeneer, W. Wegener, J. Smeets, Low friction and wear resistant a-C:H/a-Si_{1-x}C_x:H multilayer coatings, *Surf. Coating. Technol.* 86–87 (1996) 617–621, [http://dx.doi.org/10.1016/S0257-8972\(96\)02998-2](http://dx.doi.org/10.1016/S0257-8972(96)02998-2).
- [30] S. Anders, D.L. Callahan, G.M. Pharr, T.Y. Tsui, C. Singh Bhatia, Multilayers of amorphous carbon prepared by cathodic arc deposition, *Surf. Coating. Technol.* 94–95 (1997) 189–194, [http://dx.doi.org/10.1016/S0257-8972\(97\)00346-0](http://dx.doi.org/10.1016/S0257-8972(97)00346-0).
- [31] L. Wang, S. Wan, S.C. Wang, R.J.K. Wood, Q.J. Xue, Gradient DLC-based nanocomposite coatings as a solution to improve tribological performance

- of aluminum alloy, *Tribol. Lett.* 38 (2010) 155–160, <http://dx.doi.org/10.1007/s11249-010-9585-5>.
- [32] K.Y. Li, Z.F. Zhou, C.Y. Chan, I. Bello, C.S. Lee, S.T. Lee, Mechanical and tribological properties of diamond-like carbon films prepared on steel by ECR-CVD process, *Diam. Relat. Mater.* 10 (2001) 1855–1861, [http://dx.doi.org/10.1016/S0925-9635\(01\)00459-9](http://dx.doi.org/10.1016/S0925-9635(01)00459-9).
- [33] E.J. Sandoz-Rosado, O.A. Tertuliano, E.J. Terrell, An atomistic study of the abrasive wear and failure of graphene sheets when used as a solid lubricant and a comparison to diamond-like-carbon coatings, *Carbon N. Y.* 50 (2012) 4078–4084, <http://dx.doi.org/10.1016/j.carbon.2012.04.055>.
- [34] J.N. Glosli, M.R. Philpott, J. Belak, Molecular dynamics simulation of mechanical deformation of ultra-thin amorphous carbon films, *Mater. Res. Soc. Symp. Proc.* 383 (1995) 431–435.
- [35] J. Song, S. Lee, J. Lee, C.D. Yeo, Atomic degradation and wear of thin carbon films under high-speed sliding contact using molecular dynamics simulation, *Tribol. Lett.* 60 (2015), <http://dx.doi.org/10.1007/s11249-015-0577-3>.
- [36] G.T. Gao, P.T. Mikulski, J.A. Harrison, Molecular-scale tribology of amorphous carbon coatings: effects of film thickness, adhesion, and long-range interactions, *J. Am. Chem. Soc.* 124 (2002) 7202–7209.
- [37] T.-B. Ma, Y.-Z. Hu, H. Wang, Molecular dynamics simulation of shear-induced graphitization of amorphous carbon films, *Carbon* 47 (2009) 1953–1957, <http://dx.doi.org/10.1016/j.carbon.2009.03.040>.
- [38] L. Pastewka, S. Moser, M. Moseler, Atomistic insights into the running-in, lubrication, and failure of hydrogenated diamond-like carbon coatings, *Tribol. Lett.* 39 (2010) 49–61, <http://dx.doi.org/10.1007/s11249-009-9566-8>.
- [39] M.I. Baskes, J.E. Angelo, C.L. Bisson, Atomistic calculations of composite interfaces, *Model. Simul. Mater. Sci. Eng.* 2 (1999) 505–518, <http://dx.doi.org/10.1088/0965-0393/2/3A/006>.
- [40] J.E. Angelo, M.I. Baskes, Interfacial studies using the EAM and MEAM, *Interface Sci.* 63 (1996) 47–63, <http://dx.doi.org/10.1007/BF00200838>.
- [41] T. Iwasaki, H. Miura, Molecular dynamics analysis of adhesion strength of interfaces between thin films, *J. Mater. Res.* 16 (2001) 1789–1794, <http://dx.doi.org/10.1557/PROC-594-377>.
- [42] T.H. Fang, J.H. Wu, Molecular dynamics simulations on nanoindentation mechanisms of multilayered films, *Comput. Mater. Sci.* 43 (2008) 785–790, <http://dx.doi.org/10.1016/j.commatsci.2008.01.066>.
- [43] V. Prabhakaran, F.E. Talke, Wear and hardness of carbon overcoats on magnetic recording sliders, *Wear* 243 (2000) 18–24, [http://dx.doi.org/10.1016/S0043-1648\(00\)00392-6](http://dx.doi.org/10.1016/S0043-1648(00)00392-6).
- [44] D. Song, R. Kvittek, D. Schnur, Inspection of pole tip diamondlike carbon wear due to heater-induced head-disc contact, *J. Appl. Phys.* 99 (2006) 2004–2007, <http://dx.doi.org/10.1063/1.2176308>.
- [45] H. Deng, K.M. Minor, J.A. Barnard, Comparison of mechanical and tribological properties of permalloy and high moment fetan thin films for tape recording heads, *IEEE Trans. Magn.* 32 (1996) 3702–3704, <http://dx.doi.org/10.1109/20.538809>.
- [46] Z. Ma, S. Long, Y. Pan, Y. Zhou, Creep behavior and its influence on the mechanics of electrodeposited nickel films, *J. Mater. Sci. Technol.* 25 (2009) 90–94, <http://dx.doi.org/10.3321/j.issn:1005-0302.2009.01.012>.
- [47] C.P. Frick, B.G. Clark, S. Orso, A.S. Schneider, E. Arzt, Size effect on strength and strain hardening of small-scale [1 1 1] nickel compression pillars, *Mater. Sci. Eng. A* 489 (2008) 319–329, <http://dx.doi.org/10.1016/j.msea.2007.12.038>.
- [48] E. Klokholm, J.A. Aboaf, The saturation magnetostriction of permalloy films, *J. Appl. Phys.* 52 (1981) 2474–2476, <http://dx.doi.org/10.1063/1.328971>.
- [49] M.I. Baskes, Modified embedded-atom potentials for cubic materials and impurities, *Phys. Rev. B* 46 (1992) 2727–2742, <http://dx.doi.org/10.1103/PhysRevB.46.2727>.
- [50] W. Xiao, M.I. Baskes, K. Cho, MEAM study of carbon atom interaction with Ni nano particle, *Surf. Sci.* 603 (2009) 1985–1998, <http://dx.doi.org/10.1016/j.susc.2009.03.009>.
- [51] J. Tersoff, New empirical model for the structural properties of silicon, *Phys. Rev. Lett.* 56 (1986) 632–635, <http://dx.doi.org/10.1103/PhysRevLett.56.632>.
- [52] W.C.D. Cheong, L.C. Zhang, Molecular dynamics simulation of phase transformations in silicon monocrystals due to nano-indentation, *Nanotechnology* 11 (2000) 173–180, <http://dx.doi.org/10.1088/0957-4484/11/3/307>.
- [53] S. Plimpton, Fast parallel algorithms for short-range molecular dynamics, *J. Comput. Phys.* 117 (1995) 1–19, <http://dx.doi.org/10.1006/jcph.1995.1039>.
- [54] N. Wang, K. Komvopoulos, Nanomechanical and friction properties of ultra-thin amorphous carbon films studied by molecular dynamics analysis, in: *STLE/ASME 2010 Int. Jt. Tribol. Conf.* 2010, pp. 393–395.
- [55] A. Noreyan, J.G. Amar, Molecular dynamics simulations of nanoscratching of 3C SiC, *Wear* 265 (2008) 956–962, <http://dx.doi.org/10.1016/j.wear.2008.02.020>.
- [56] Y. Gao, C. Lu, N.N. Huynh, G. Michal, H.T. Zhu, A.K. Tieu, Molecular dynamics simulation of effect of indenter shape on nanoscratch of Ni, *Wear* 267 (2009) 1998–2002, <http://dx.doi.org/10.1016/j.wear.2009.06.024>.
- [57] R. Wood, Future hard disk drive systems, *J. Magn. Magn. Mater.* 321 (2009) 555–561, <http://dx.doi.org/10.1016/j.jmmm.2008.07.027>.
- [58] R. Komanduri, N. Chandrasekaran, L.M. Raff, MD simulation of indentation and scratching of single crystal aluminum, *Wear* 240 (2000) 113–143, [http://dx.doi.org/10.1016/S0043-1648\(00\)00358-6](http://dx.doi.org/10.1016/S0043-1648(00)00358-6).
- [59] Y. Yan, T. Sun, S. Dong, Y. Liang, Study on effects of the feed on AFM-based nano-scratching process using MD simulation, *Comput. Mater. Sci.* 40 (2007) 1–5, <http://dx.doi.org/10.1016/j.commatsci.2006.10.020>.
- [60] Y.C. Liang, J.X. Chen, M.J. Chen, Y.L. Tang, Q.S. Bai, Integrated MD simulation of scratching and shearing of 3D nanostructure, *Comput. Mater. Sci.* 43 (2008) 1130–1140, <http://dx.doi.org/10.1016/j.commatsci.2008.03.012>.
- [61] Q.K. Li, M. Li, Atomic scale characterization of shear bands in an amorphous metal, *Appl. Phys. Lett.* 88 (2006) 98–101, <http://dx.doi.org/10.1063/1.2212059>.
- [62] X.W. Zhou, J.A. Zimmerman, E.D. Reedy, N.R. Moody, Molecular dynamics simulation based cohesive surface representation of mixed mode fracture, *Mech. Mater.* 40 (2008) 832–845, <http://dx.doi.org/10.1016/j.mechmat.2008.05.001>.
- [63] T. Sato, T. Saito, S. Fujita, Mechanism of diamond-like carbon (DLC) delamination under rolling contact condition, *Tribol. Online* 3 (2008) 337–341, <http://dx.doi.org/10.2474/trol.3.337>.
- [64] M.R. Price, A. Ovcharenko, R. Thangaraj, B. Raeymaekers, Deformation of ultra-thin diamond-like carbon coatings under combined loading on a magnetic recording head, *Tribol. Lett.* 57 (3) (2015) 1–9, <http://dx.doi.org/10.1007/s11249-014-0449-2>.
- [65] H. Holleck, V. Schier, Multilayer PVD coatings for wear protection, *Surf. Coating. Technol.* 76–77 (1995) 328–336, [http://dx.doi.org/10.1016/0257-8972\(95\)02555-3](http://dx.doi.org/10.1016/0257-8972(95)02555-3).
- [66] G. Voronoi, Nouvelles applications des parametres continus a la theorie des formes quadratiques, *J. Reine. Angew. Math.* 134 (1908) 198–287, <http://dx.doi.org/10.1515/crll.1909.136.67>.
- [67] W. Yang, S. Rehman, X. Chu, Y. Hou, S. Gao, Transition metal (Fe, Co and Ni) Carbide and nitride Nanomaterials: Structure, chemical synthesis and applications, *ChemNanoMat* 13 (2015) 76–398, <http://dx.doi.org/10.1002/cnma.201500073>.
- [68] Z.L. Schaefer, K.M. Weeber, R. Misra, P. Schiffer, R.E. Schaak, Bridging hcp-Ni and Ni₃C via a Ni₃C 1-x solid solution: tunable composition and magnetism in colloidal nickel carbide nanoparticles, *Chem. Mater.* 23 (2011) 2475–2480, <http://dx.doi.org/10.1021/cm200410s>.
- [69] M.R. Price, A. Ovcharenko, B. Raeymaekers, Qualitative evaluation of ultra-thin multi-layer diamond-like carbon coatings using molecular dynamics nano-indentation simulations, *Tribol. Lett.* 62 (2016) 1–10, <http://dx.doi.org/10.1007/s11249-016-0655-1>.
- [70] D.M. Follstaedt, J.A. Knapp, S.M. Myers, Mechanical properties of ion-implanted amorphous silicon, *J. Mater. Res.* 19 (2004) 338–346, <http://dx.doi.org/10.1557/jmr.2004.19.1.338>.
- [71] C. Casiraghi, J. Robertson, A.C. Ferrari, Diamond-like carbon for data and beer storage, *Mater. Today* 10 (2007) 44–53, [http://dx.doi.org/10.1016/S1369-7021\(06\)71791-6](http://dx.doi.org/10.1016/S1369-7021(06)71791-6).
- [72] J. Veverkova, S.V. Hainsworth, Effect of temperature and counterface on the tribological performance of W-DLC on a steel substrate, *Wear* 264 (2008) 518–525, <http://dx.doi.org/10.1016/j.wear.2007.04.003>.
- [73] K.L. Choy, E. Felix, Functionally graded diamond-like carbon coatings on metallic substrates, *Mater. Sci. Eng. Struct. Mater. Prop. Microstruct. Process* 278 (2000) 162–169, [http://dx.doi.org/10.1016/S0921-5093\(99\)00569-9](http://dx.doi.org/10.1016/S0921-5093(99)00569-9).
- [74] C. Charitidis, S. Logothetidis, M. Gioti, A comparative study of the nano-scratching behavior of amorphous carbon films grown under various deposition conditions, *Surf. Coating. Technol.* 125 (2000) 201–206, [http://dx.doi.org/10.1016/S0257-8972\(99\)00546-0](http://dx.doi.org/10.1016/S0257-8972(99)00546-0).
- [75] S. Zhang, X.L. Bui, Y. Fu, D.L. Butler, H. Du, Bias-graded deposition of diamond-like carbon for tribological applications, *Diam. Relat. Mater.* 13 (2004) 867–871, <http://dx.doi.org/10.1016/j.diamond.2003.10.043>.
- [76] C. Mathioudakis, P. Kelires, Y. Panagiotatos, P. Patsalas, C. Charitidis, S. Logothetidis, Nanomechanical properties of multilayered amorphous carbon structures, *Phys. Rev. B* 65 (2002) 1–14, <http://dx.doi.org/10.1103/PhysRevB.65.205203>.
- [77] D.R. McKenzie, R.N. Tarrant, M.M.M. Bilek, T. Ha, J. Zou, W.E. McBride, D.J.H. Cockayne, N. Fujisawa, M.V. Swain, N.L. James, J.C. Woodard, D.G. McCulloch, Multilayered carbon films for tribological applications, *Diam. Relat. Mater.* 12 (2003) 178–184, [http://dx.doi.org/10.1016/S0925-9635\(03\)00020-7](http://dx.doi.org/10.1016/S0925-9635(03)00020-7).
- [78] N.W.-D. John Towns, Timothy Cockerill, Maytal Dahan, Ian Foster, Kelly Gaiher, Andrew Grimshaw, Victor Hazelwood, Scott Lathrop, Dave Lifka, Gregory Peterson, Ralph Roskies, J. Ray Scott, XSEDE: accelerating scientific Discovery, *Comput. Sci. Eng.* 16 (2014) 16–74.
- [79] J. Li, AtomEye: an efficient atomistic configuration viewer, *Model. Simul. Mater. Sci. Eng.* 11 (2003) 173–177, <http://dx.doi.org/10.1088/0965-0393/11/2/305>.